Simulation-Based Optimization of the Acoustoelectric Hydrophone for Mapping an Ultrasound Beam

Zhaohui Wang[a,b*], Pier Ingram[a], Ragnar Olafsson[a], Charles L. Greenlee[c], Robert A. Norwood[c], Russell S. Witte[a,c]
[a]Department of Radiology, University of Arizona, Tucson, AZ 85724
[b]Department of Electrical and Computer Engineering, University of Arizona, Tucson, AZ 85724
[c]Department of Optical Sciences, University of Arizona, Tucson, AZ 85724

ABSTRACT

Most single element hydrophones depend on a piezoelectric material that converts pressure changes to electricity. These devices, however, can be expensive, susceptible to damage at high pressure, and/or have limited bandwidth and sensitivity. The acousto-electric (AE) hydrophone is based on the AE effect, an interaction between electrical current and acoustic pressure generated when acoustic waves travel through a conducting material. As we have demonstrated previously, an AE hydrophone requires only a conductive material and can be constructed out of common laboratory supplies to generate images of an ultrasound beam pattern consistent with more expensive hydrophones. The sensitivity is controlled by the injected bias current, hydrophone shape, thickness and width.

In this report we describe simulations aimed at optimizing the design of the AE hydrophone with experimental validation using new devices composed of a resistive element of indium tin oxide (ITO). Several shapes (e.g., bowtie and dumbbell) and resistivities were considered. The AE hydrophone with a dumbbell configuration achieved the best beam pattern of a 2.25MHz ultrasound transducer with lateral and axial resolutions consistent with images generated from a commercial hydrophone (Onda Inc.). The sensitivity of this device was ~2 nV/Pa. Our simulations and experimental results both indicate that designs using a combination of ITO and gold (ratio of resistivities = ~18) produce the best results. We hope that design optimization will lead to new devices for monitoring ultrasonic fields for biomedical imaging and therapy, including lithotripsy and focused ultrasound surgery.

Keyword: Acousto-electric, hydrophone, ultrasound, current density distribution, mapping, relative resistivity, ultrasound detectors, ablation therapy

1. INTRODUCTION

The simple, rapid and accurate estimation of the acoustic field is very important in the clinical ultrasound applications expanding from imaging to focused ultrasound therapy for tumor ablation. The traditional acoustic measuring devices like fiber, membrane, and needle hydrophones are available depending on the application. These devices, however, are limited by their specific physical properties, often leading to limited bandwidth for detecting the acoustic signal, high cost of fabrication, and/or susceptible to damage under high pressure.

The AE effect is based on the interaction between a propagating acoustic wave and charged particles in a material. Previous hydrophones based on the acousto-electric (AE) effect ([1], [2]) relied on piezoelectric materials embedded between two semiconductors to measure ultrasound pressure field. These AE devices had poor sensitivity and could only detect the power of the signal (no phase information). We have shown theoretically and experimentally, ultrasound current source density imaging (UCSDI) can map the impedance and current flow in samples in three dimensions and at high spatial resolution ([2], [3], [4]). In addition, it depends on the distribution of current density, relative resistivity between center sensing area and the rest conductive area. It can generate images of an ultrasound beam pattern consistent with more expensive hydrophones. As an alternative to conventional hydrophones, a new design based on the AE effect has attractive attributes not typically observed in other hydrophones: simple construction, low cost, decent sensitivity, resilience to damage at high intensity ultrasound field, and potentially wider bandwidth and improved sensitivity. The acousto-electric hydrophone [5] can use practically any conductive material. As a result, they are not limited to piezo-materials, possibly leading to novel designs at low cost. This new device was composed of a center semi-conducting

* zwang@email.arizona.edu; phone 1 520 626 1936; www.u.arizona.edu/~rwitte/

Medical Imaging 2010: Ultrasonic Imaging, Tomography, and Therapy, edited by Jan D'hooge, Stephen A. McAleavey,
Proc. of SPIE Vol. 7629, 76290Q · © 2010 SPIE · CCC code: 1605-7422/10/$18 · doi: 10.1117/12.844651

element of indium tin oxide (ITO) and the rest area of ITO or gold (figure 1(b)). The transducer center frequency determines the optimal size of the sensitivity zone. Resistivity $\rho_0 = \rho_0(x, y, z)$ can be variable on the surface of AE hydrophone, and the relative resistivity is defined as the ratio of resistivity of the center area over that of the rest conductive area. The performance of bowtie hydrophone can be improved by increasing relative resistivity. Rel is relative resistivity between the center area and conductive area; Rel=1 means the center area is the same material as the rest conductive area. The larger Rel value, the higher the resistivity of center conductive area will be.

MEMS techniques were used to fabricate the AE hydrophones with fine control [6]. In this report, the simulation aims at optimizing the design of the AE hydrophone with experimental validation. Multi-dimensional Fourier-based reconstructions are also used to optimize the simulation speeds. Several shapes (e.g., bowtie and dumbbell) and a variety of relative resistivities (Rel) were investigated to optimize the design of AE hydrophone. The sensitivity and harmonic analysis were also made to investigate the effect of thickness and width of AE hydrophone. The simulated curves are also used to calibrate the real relative resistivity from the experimental data.

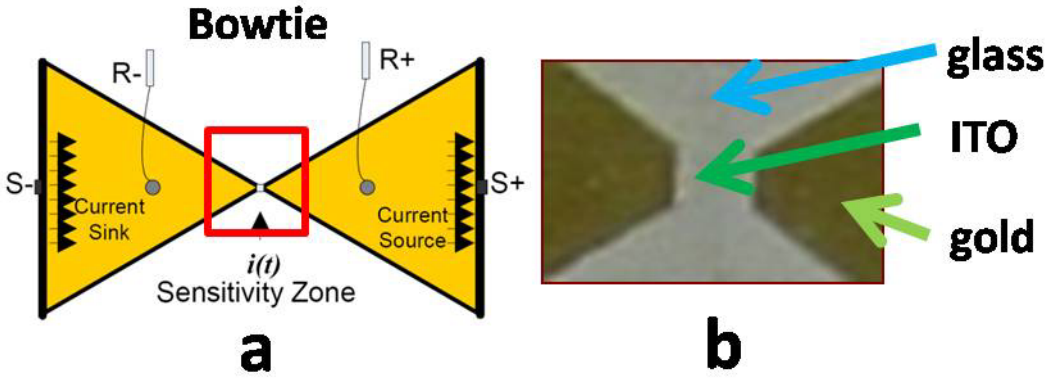

Figure 1. The structure of bowtie AE hydrophone. (a) Current is injected from electrode S+ to S-, the AE signal is obtained from the electrodes R+ and R-. (b) The bowtie AE hydrophone is built on glass substrate, the sensitive zone material is ITO, and the rest area is made of gold.

2. METHODS

2.1. Experimental setup

In figure 1(a) and figure 2(a), one pair of electrodes was used to inject current (alternating current, typically ~200 Hz) and another pair was used for detecting the AE signal. In this example, gold leads in the shape of a bow-tie converged to the resistive element in the center of the hydrophone. The maximum (90 degree) or minimum (270 degree) current injection was synchronized with a square-wave pulser/receiver (Olympus NDT, Model 5077PR), which excited a single-element focused transducer (2.25MHz, f/1.8, focal length). Common mode noise can be reduced by subtracting the two AE signals with opposite phases. The AE signals, as well as simultaneously acquired pulse echo signals (PE) received by the transducer, were amplified, band-pass filtered and captured with a fast 12-bit acquisition board (Signatec, Inc.), and pulse echo (PE) signal is the radio frequency (RF) signal received by transducer. A 2-D raster scan provided a 3D beam pattern based on the AE signals that was further compared with simulations generated in MATLAB™ (see below).

A variety of AE hydrophones were designed, constructed, simulated and tested based on a structure with a small resistive element (e.g., indium tin oxide with a gap as small as 75 μm). Four primary factors were investigated during the final design of the AE hydrophone: shape, width, thickness and relative resistivity. Three different shapes: triangular bowtie, circular and rectangular dumbbells determine the current distribution in the lead field. This design had the center area ("sensitivity zone") with one resistivity and the remaining area with the same or different resistivity connecting to the lead wires.

2.2. Sensitivity and SNR analysis

The commercial Onda hydrophone (HGL-0200) works as a standard to calibrate the pressure received by acousto-electric hydrophone. The pressures at the focus under different pressures were obtained by sweeping the transducer

voltage from high to low. The Onda hydrophone was operated with the same hardware and software filtering characteristics as we used during the AE hydrophone experiments to maintain consistency among experiments and enable direct comparisons.

Each AE hydrophone was evaluated at different pressures and injected bias voltages. The transducer pressure is determined by the input voltage to the 2.25 MHz ultrasound transducer (100 V to 400 V, which was converted to pressure based on measurement with a calibrated hydrophone (Onda). At each pressure, the bias voltage through the AE hydrophone is determined by the applied voltage of the signal generator, variable from high (20 V) to low (0 V), and the lowest is referred to the noise (or "control") signal. The peak-peak value of filtered data is used for the calculation of sensitivity. The sensitivity of an AE hydrophone can be calculated by dividing the detected voltage by the transducer pressure.

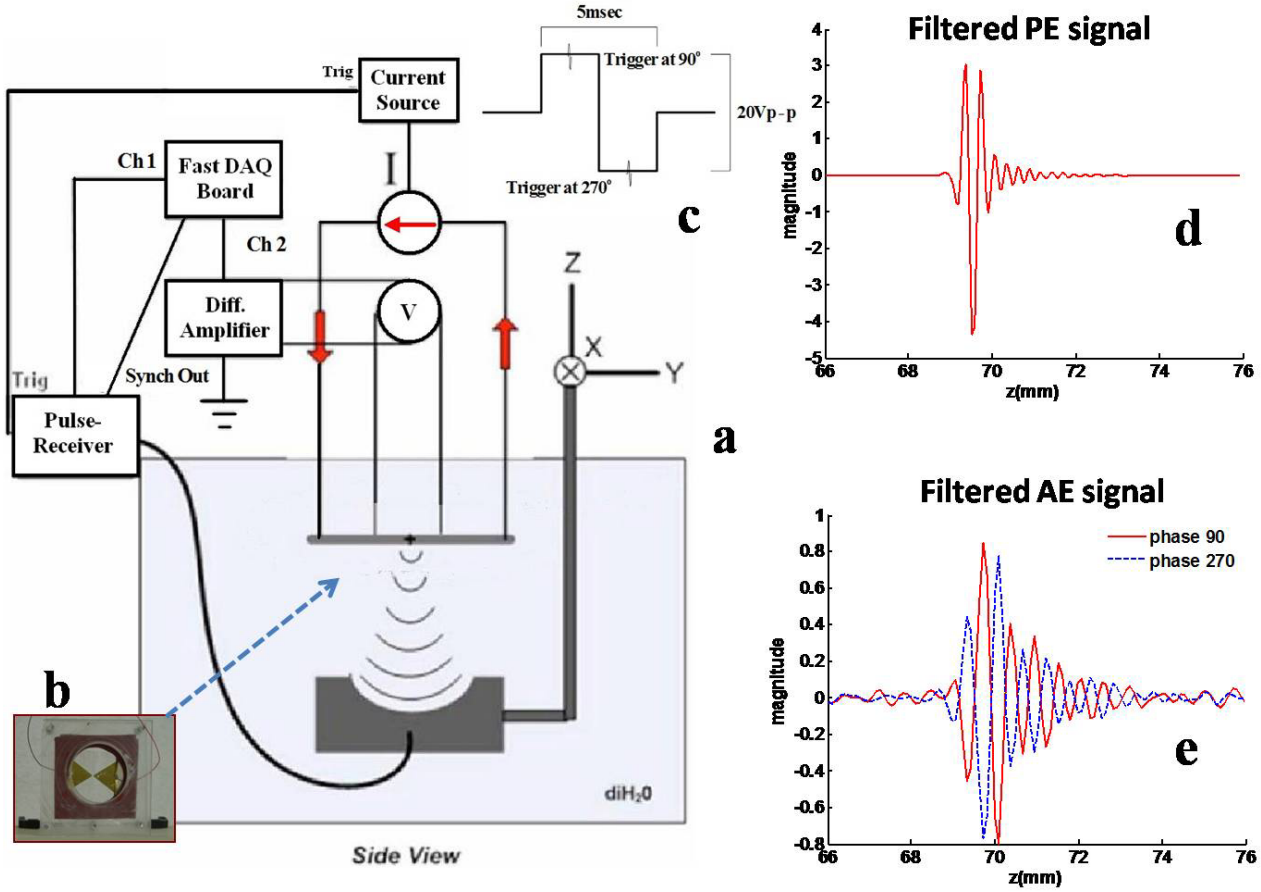

Figure 2. Experimental setup for characterizing the hydrophone. A current source injected a 200 Hz rectangular waveform into the hydrophone. AE signals were acquired at the maxima (90 degree) and minima (270 degree) of the waveform. In the top right is the pulse echo (PE) signal, and in the bottom right are the acousto-electric (AE) signals acquired at the maxima (phase 90) and minima (phase 270) of the current waveform. Common mode noise is further reduced by subtracting the two AE signals with opposite phase.

2.3. Simulation

It is assumed that single element 2.25MHz concave transducer is excited by a square pulse obtained from the signal generator, and the ultrasound pressure field $b(x, y, z)$ can be created by convolving spatial impulse response in the Field II simulation software ([7], [8]).

The electric simulations were based on lead field theory. The current density distribution $J(x, y, z)$ and electric fields were simulated using MATLAB's partial differential equation toolbox. The electrodes (including injecting and detecting) were defined as Dirichlet boundary conditions, and the other boundaries are Neumann boundary conditions. Finite

element analysis was used to simulate the current density distribution in a pure resistive sample having the same geometry as the experimental one. The equation appropriate for a finite element simulation is the Poisson equation $-\nabla \cdot (\sigma \nabla \varphi) = \rho$ with the Neumann boundary condition $\mathbf{J} \cdot \mathbf{n} = 0$, where $\rho = \rho_0[\delta(\mathbf{r} - \mathbf{r_1}) - \delta(\mathbf{r} - \mathbf{r_2})]$ (see figure 3(a)) is a dipole with point charges located at positions $\mathbf{r_1}$ and $\mathbf{r_2}$ within the sample or on the boundaries, to account for an injected current or detecting electrodes. Adaptive mesh refinement algorithm was also used to improve the accuracy of the current density distribution. Figure 3(a) shows the refined mesh for bowtie hydrophone. After computation, the electric voltage and mesh information were downloaded from pdetool. The current density can be calculated by $\boldsymbol{J} = \sigma \nabla V$, and make sure $\mathbf{J} \cdot \mathbf{n} = 0$ on the edge of hydrophone. In figure 3(b), the current density is highest at the center and electrode areas, and decreases quickly away these areas.

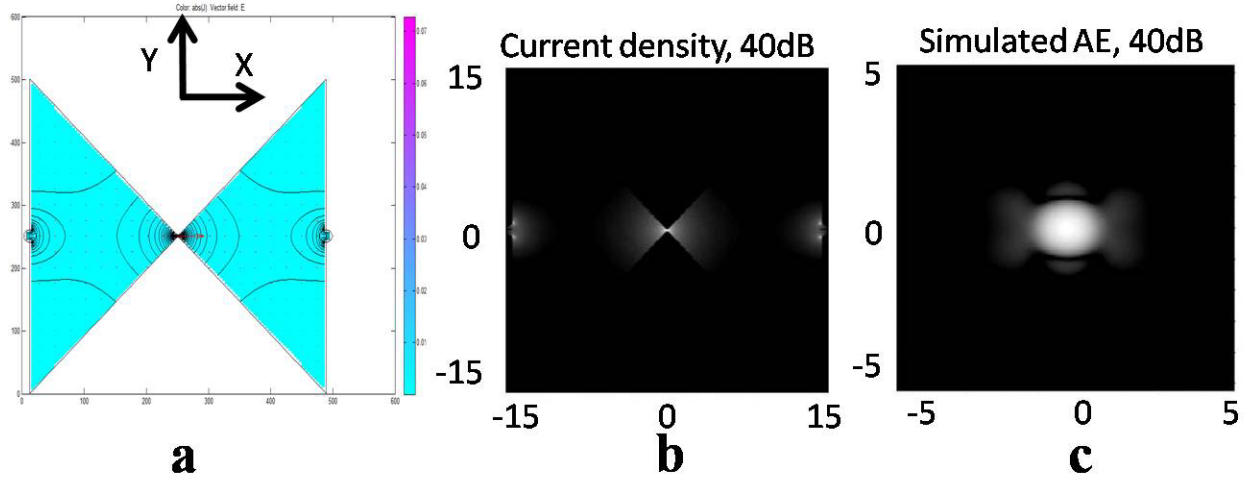

Figure 3. Acousto-electric (AE) signal induced by the 2.25 MHz transducer on a bowtie hydrophone design with center gap of 200μm. Simulations are coincident with the experimental result. (a) Current distribution and electric field simulated by conductive media DC application in MATLAB partial differential equation toolbox, where two electrodes are defined by Dirichlet boundary conditions, the other by Neumann boundary conditions. (b) Current density distribution of lead field is calculated based on the simulated potential in electric field and mesh information. (c) Simulated AE envelope dB plot at the focus for bowtie hydrophone, whose center is 200μm*200μm. The dimensional unit for (b) and (c) is mm.

To avoid the interference of noise, the AE signal V_i^{AE} at (x_0, y_0, z_0) is applied band-pass filter with the same center frequency of transducer ([2], [5]). In figure 4, if the center of beam pattern points at C(x_0, y_0, z_0), then any point P in the ultrasound pressure field (x, y, z) can be described in the electric field as (x+x_0, y+y_0, z+z_0).

$$V_i^{AE}(x_0, y_0, z_0, t) = -P_0 \iiint K_I \rho_0 \left(\tilde{J}_i^L \cdot J^I\right)(x + x_0, y + y_0, z + z_0) \left[\int b(x, y, z) a\left(t - \frac{z}{c}\right) h(t' - t) dt'\right] dxdydz \quad (1)$$

where P_0 is the amplitude of the pressure pulse, $K_I = K_I(x, y, z)$ is the interaction constant whose value is of the order of 10^{-9}Pa^{-1}, $\rho = \rho(x, y, z)$ is the resistivity, $J(x, y, z)$is current distribution of hydrophone, $b(x, y, z)$ is the ultrasound beam pattern, $a\left(t - \frac{z}{c}\right)$ is the pulse waveform, $h(t)$is the band-pass filter with the same center frequency of transducer.

As $K_I = K_I(x, y, z)$, $\rho_0 = \rho_0(x, y, z)$ both depend on the material properties, they can be combined together with $J(x, y, z)$, so that

$$w_i(x, y, z) = K_I(x, y, z)\rho_0(x, y, z)\left(\tilde{J}_i^L \cdot J^I\right)(x, y, z)$$

$$p(x, y, z, t) = b(x, y, z) a\left(t - \frac{z}{c}\right)$$

where $p(x, y, z, t)$ is the ultrasound wave field at time t, then $V_i^{AE}(x_0, y_0, z_0, t)$ can be calculated quickly by Foureir transform.

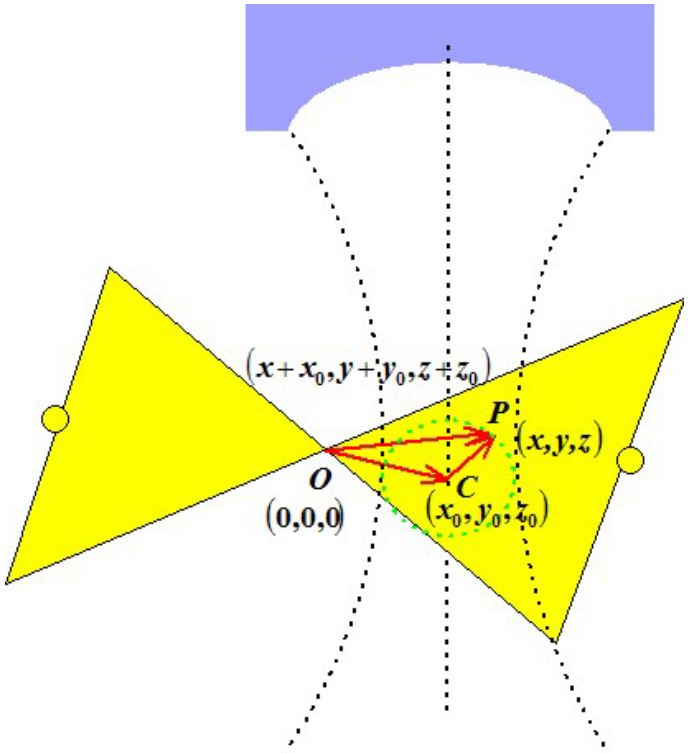

Figure 4. Schematic of the acousto-electric effect on the bowtie AE hydrophone. Coordinate center O$(0,0,0)$ is at the center of sensitive zone. Transducer center is C(x_0, y_0, z_0), and any point P in the ultrasound pressure field (x, y, z) can be described in the electric field as $(x + x_0, y + y_0, z + z_0)$.

$$V_i^{AE}(x_0,y_0,z_0,t) = -P_0 \iiint w_i(x+x_0,y+y_0,z+z_0)\left[\int p(x,y,z,t)h(t'-t)dt'\right]dxdydz$$
$$= -P_0 F^{-1}{}_{x,y,z}\left\{W_i^*(k_x,k_y,k_z)F_{k_x,k_y,k_z}\left[F^{-1}{}_t\left(P(x,y,z,k)H(k)\right)\right]\right\} \quad (2)$$

where the $F^{-1}{}_{x,y,z}$ is 3D inverse Fourier transform over (k_x, k_y, k_z), W is the x-y-z 3D Fourier transform of $w(x,y,z)$, W^* is the conjugate of W, F_{k_x,k_y,k_z} is 3D Fourier transform over (x,y,z), $F^{-1}{}_t$ is the inverse Fourier transform over k, $P(x,y,z,k)$ is 1D Fourier transform of $p(x,y,z,t)$ over t, $H(k)$ is the Fourier transform of $h(t)$.

A complete map of an ultrasound beam pattern can, therefore, be obtained by scanning the ultrasound beam along the lateral and level direction over the surface of AE hydrophone. If the thickness of the AE hydrophone is thin as compared to the ultrasound wavelength λ, the solution reduces to a double integral over the lateral and level direction at the depth of the hydrophone. If the AE hydrophone is oriented on the x-y surface plane, $w(x+x_0,y+y_0,z+z_0)$ becomes $w(x+x_0,y+y_0)$, then

$$V_i^{AE}(x_0,y_0,t) = -P_0 \iiint w_i(x+x_0,y+y_0)\left[\int p(x,y,t)h(t'-t)dt'\right]dxdy$$
$$= -P_0 F^{-1}{}_{x,y}\left\{W_i^*(k_x,k_y)F_{k_x,k_y}\left[F^{-1}{}_t\left(P(x,y,k)H(k)\right)\right]\right\} \quad (3)$$

Dimensional analysis over thickness and width can be done along cross-section (x-z plane), $w(x+x_0,y+y_0,z+z_0)$ becomes $w(x+x_0,z+z_0)$, J^I is assumed constant and independent of position (x,z) over the cross-section, and its unit vector is the same as $\tilde{J}_i^L$.

$$V_i^{AE}(x_0,z_0,t) = -P_0 \iiint w_i(x+x_0,z+z_0)\left[\int p(x,z,t)h(t'-t)dt'\right]dxdz$$
$$= -P_0 F^{-1}{}_{x,z}\left\{W_i^*(k_x,k_z)F_{k_x,k_z}\left[F^{-1}{}_t\left(P(x,z,k)H(k)\right)\right]\right\} \quad (4)$$

where $w_i(x,z) = K_I(x,z)\rho_0(x,z)J^I$. As the connection between the electrode and the slab is usually the small area around the center of the cross-section, the detected V_i^{AE} can be the average value over the area around the center. For the convenience, the connection can be assumed one point on the center, then detected V_i^{AE} is the value on the center.

A 3D simulation of the magnitude of the AE signal was created by convolving the ultrasound field (simulated with Field II™) with the current density distribution in the lead field, and this convolution can be accelerated using a Fast Fourier Transform algorithm. Combining the ultrasound beam and bowtie electric field, we get the simulated result of figure 3(c) (or figure 5(a1-a3) and figure 5(b1-b3)).

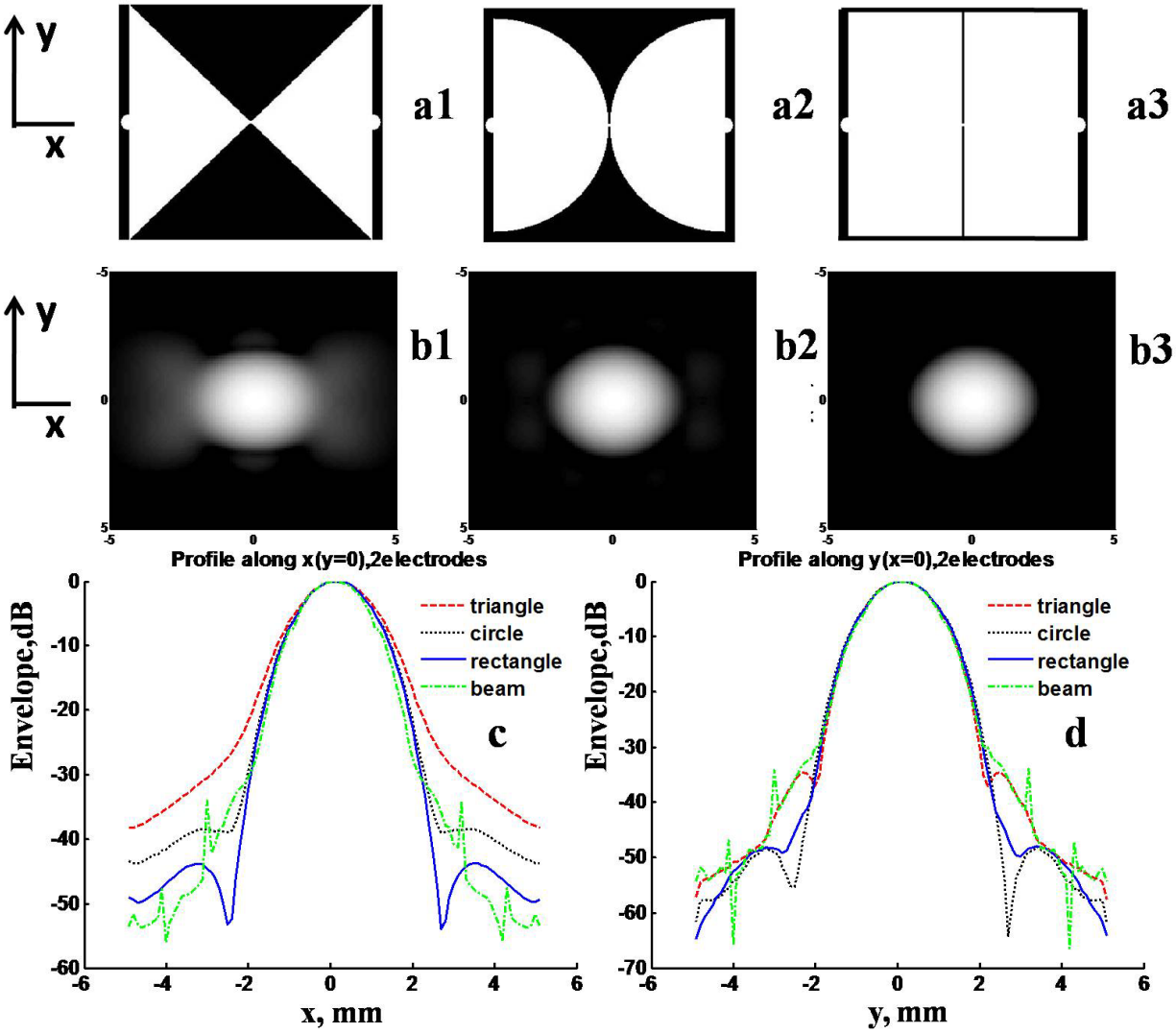

Figure 5. Simulation results with different shapes. Acousto-electric (AE) signals induced by a 2.25 MHz transducer are simulated with three different hydrophone designs. The three designs have different shapes: triangular bowtie, circular and rectangular dumbbells, with center area about 200µm*200µm. It is assumed that the entire material has identical resistivity. (a1-a3) Three designs with different shapes: bowtie (triangle, a1), dumbbell (circle, a2, and rectangle, a3). (b1-b3) Simulated AE signal along x-y plane on the focus for bowtie (b1), circular (b2) and rectangular (b3) dumbbells. (b1) has highest sidelobe and biggest beam width along x direction. (c) AE profile on the center along x horizontal direction; (d) Center profile along y direction. The AE hydrophone with rectangular shape has the smallest full width at half maximum (FWHM) and lowest sidelobe along the x direction. In (d), the circular dumbbell has the lowest sidelobe, but the dB value of rectangular shape drops the fastest, and at more than 4.5mm away from the center, its dB value is the smallest. 'Beam' is simulated transducer beam pattern, created by the convolution of ultrasound field with AE signal obtained by Onda hydrophone. Field II™ was used for all ultrasound simulations.

3. RESULTS AND DISCUSSION

3.1. Effect of hydrophone shape

The shape of hydrophone is critical for determining the current distribution and ultimately the selectivity and sensitivity of the AE hydrophone for mapping the ultrasound beam pattern, as depicted in figure 5(b1-b3). The AE hydrophone with rectangular shape has the smallest full width at half maximum (FWHM) and lowest sidelobe along the lateral short axis (x) direction (figure 5(c)). Along the long axis (y) direction (figure 5(d)), the circular dumbbell has the lowest sidelobe, but the dB value of rectangular shape drops fastest, and at more than 4.5mm from the center, its dB value is lowest. The x-y cross-section on the focus is elliptical for bowtie, but circular for circular or rectangular dumbbell.

These analyses can further be supported form the 3D data in figure 6(a), (b) and (c). In x-z image, the two holes on the focus of ideal beam, where the sidelobes locate, split into four holes in bowtie hydrophone (Rel=1) before or behind of the focus, so there is no sidelobe for bowtie in figure 5(c). Therefore bowtie (Rel=1) is not axial symmetrical and distorts the beam pattern heavily, but dumbbell is axial symmetrical, and circular along cross-section.

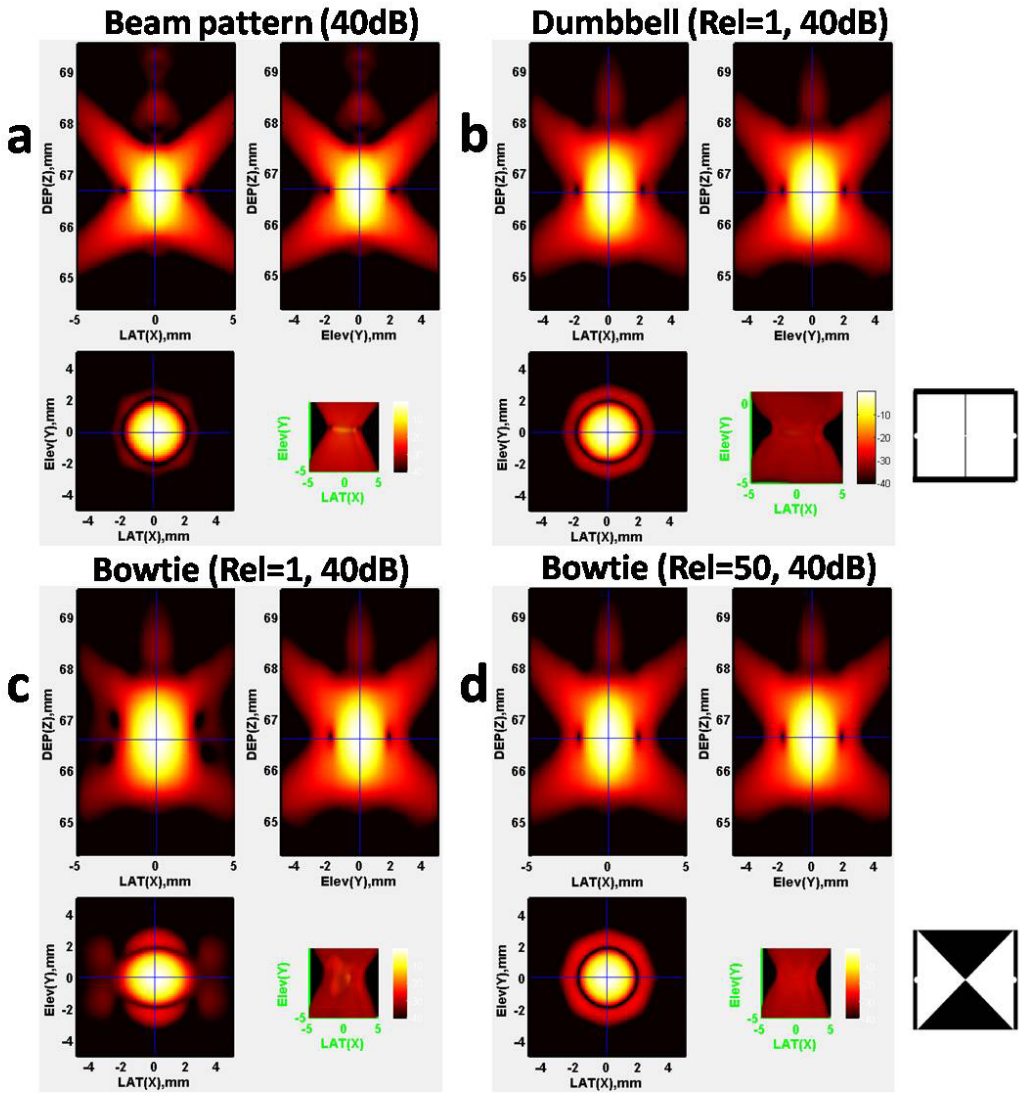

Figure 6. 3D cross-sectional 40dB envelope images of simulated data show the comparison between beam pattern (a), dumbbell (Rel=1, b), bowtie (Rel=1, c) and bowtie (Rel=50, d) hydrophones. Each group contains X-Z, Y-Z and X-Y cross-sectional 40dB envelope, the horizontal and vertical crossing lines mark the position of three coordinates.

3.2. Effect of material relative resistivity

Figure 6(a) is the ideal beam pattern of 40dB envelope 3D cross-sectional display at the focus center, in x-z cross-section, the center two holes determines the first sidelobe position. For bowtie hydrophone, if Rel=1 (figure 6(c)), the center two holes are separated into four holes, and the x-y cross-section is elliptical, but if Rel=50 (figure 6(d)), the x-y cross-section is sphere and close to the idea shape in figure 6(a). Bowtie (Rel=50) hydrophone shows almost the same performance as dumbbell (Rel=1) hydrophone (figure 6(b)).

It is easier to make bowtie shape than to create a clean long thin gap for dumbbell hydrophone, especially tiny size about several um for high frequency transducer. Bowtie hydrophone with high Rel value needs one extra procedure to create the center area. Therefore, there is tradeoff between the fabrication complexity and difficulty.

3.3. Effect of thickness

In figure 7(a), the sensitivity increases with thickness until more than half wavelength of transducer, then the sensitivity keeps constant. The linear range of sensitivity over thickness is from 0 to half wavelength. The thickness have important effect of the spectrum of AE signal, when thickness increases from 0, the 1st harmonic magnitude decreases and reaches lowest at thickness $= \frac{\lambda}{2}$. If thickness $> \frac{\lambda}{2}$, the 1st harmonic begin increasing. If thickness is larger than λ, the harmonic components move leftward, putting the center frequency of main lobe smaller. In the time domain, the two top peaks begin moves in opposite direction, and the maximum does not change. So the source of spectrum distortion mostly comes from the thickness.

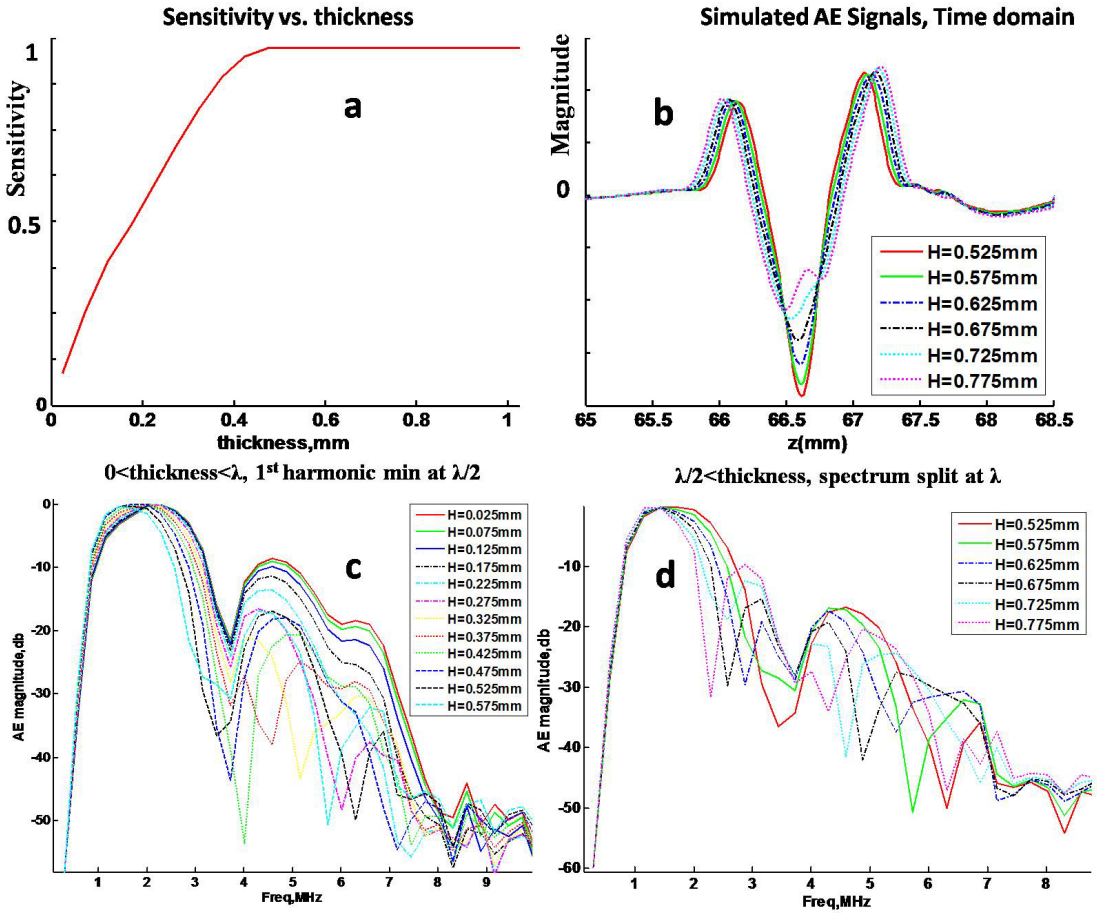

Figure 7. Simulation results: the thickness analysis for the AE hydrophone is made by ranging thickness from 0.025mm to 0.775mm. (a) is the sensitivity plot, (b) is the simulated AE A-lines at the center of cross-section, (c) is the spectrum of the simulated AE A-lines for thickness around half wavelength, (d) is spectrum of the simulated AE A-lines for thickness higher than half wavelength. The center frequency of transducer is 2.25MHz, and its wavelength is about 657μm.

3.4. Effect of lateral width

As the x-z cross-section of center area is uniform, V_i^{AE} can be simulated along cross-section, and both width and thickness are important for the detected AE voltage. Based on equation (3) , the V_i^{AE} can be obtained by applying inverse Fourier transform of the product between current distribution and ultrasound field in the frequency domain.

In [4] figure 7, the transducer center frequency is 2.25MHz (wavelength is about 658um) and the width of slab was changed from 0.025mm to 7.025mm. In time domain, the peak positions of V_i^{AE} is maintained constant, and the sensitivity reaches maximal value when lateral width is larger than the beam size. The sidelobe position does not change, and decreases and converges to steady value. For the frequency spectrum of AE signal, the magnitude of the higher harmonic components decreases and converges to a steady value.

3.5. Sensitivity and SNR analysis

Figure 8 and figure 9 are the analysis based on the experimental data of dumbbell (Rel=1) hydrophone. In figure 9, if the unit of sensitivity is defined as nV/Pa, the sensitivity increases with the current, about 0.4nV/Pa for a 20V signal. As it is difficult to tell the effect of current in sensitivity, it is further divided by the current, nV/Pa/V, which is referred as "normalized sensitivity," or bias voltage corrected. In figure 9(c), the normalized sensitivity becomes constant when the injected current is bigger than 4 V; from figure 9(d), if current is bigger than 4V, the normalized sensitivity is independent of transducer pressure. Therefore, the sensitivity is linearly determined by the injected current. As $\widetilde{J}_i^L$ is in the same direction of J^I on the center conductive area, $w_i(x,y) = K_I(x,y)\rho_0(x,y)\left(\widetilde{J}_i^L \cdot J^I\right) = K_I(x,y)\rho_0(x,y)|J^I|$. The sensitivity can be controlled by the injected current, hydrophone width and thickness.

SNR (signal to noise ratio) is defined as the ratio of the measured peak-peak value of filtered data between the signal and the noise (signal source is 0 volt). In this experiment, the data at 1 V current is assumed to be noise signal. SNR increases linearly with increased injected current (figure 8(a)) and transducer pressure (figure 8(b)). Therefore, SNR can be improved by increasing the bias injected current.

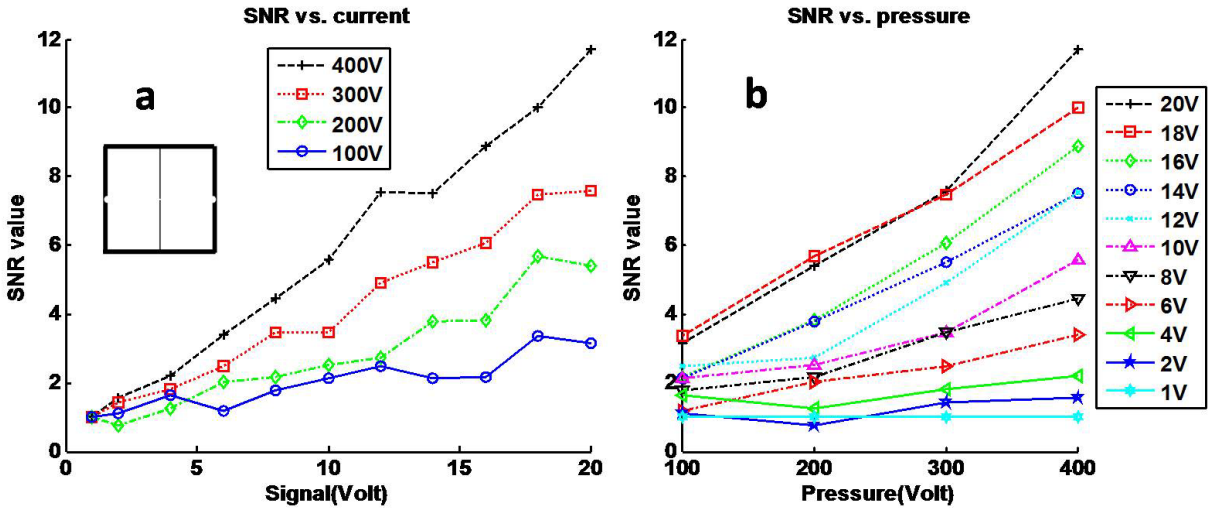

Figure 8. SNR analysis shows the effect of injected current and transducer pressure. The sensitive zone on the center of rectangular dumbbell (Rel=1) is 75μm*75μm. The center frequency of transducer is 2.25MHz.

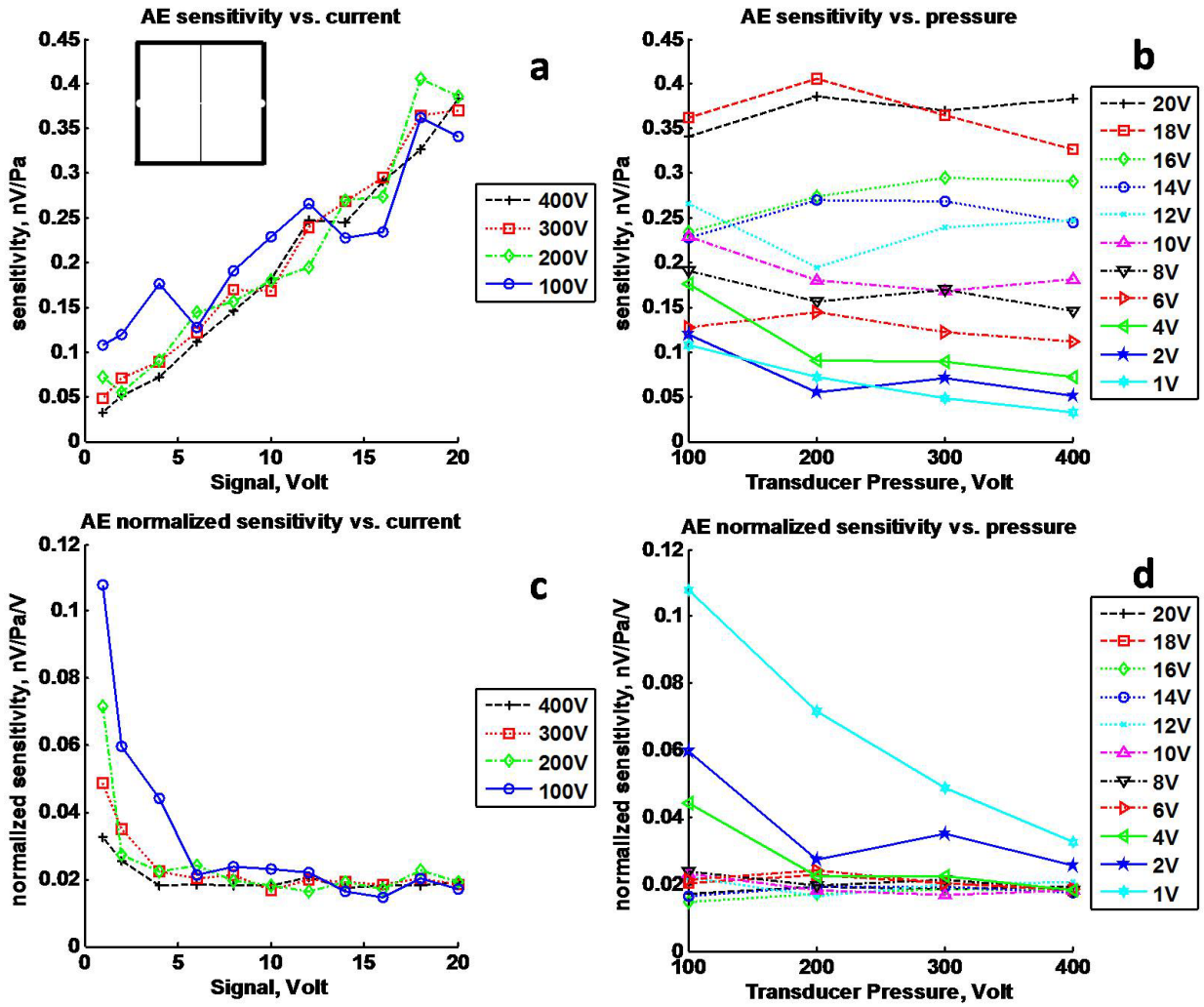

Figure 9. Sensitivity (a and b) and normalized sensitivity (c and d) analysis of dumbbell (Rel=1) hydrophone show the effect of injected current and transducer pressure. The sensitive zone on the center is 75μm*75μm. The center frequency of transducer is 2.25MHz.

3.6. Calibration of relative resistivity

In this case, ITO ($5*10^{-4}$~$5*10^{-5}$Ω·cm) fills the center area, and gold (Au, $2.4*10^{-6}$Ω·cm) covers the rest area; the ratio of the resistivity of ITO to Au is in the range of 20 to 100. The relative resistivity of ITO/Au can be calibrated using the simulated and experimental data for bowtie hydrophone. Relative resistivity does not affect the center profile or beam width along the y direction (figure 10(b)), so only the profile along the x direction is used to approximate the relative resistivity of ITO/Au. In figure 10(a), when Rel is increased from 1 to 50, the sidelobe decreases and converges to the ideal beam profile. At 21dB (figure 10(c)), if the relative resistivity of ITO/Au is higher than 18, the beam width becomes equivalent to the experimental result (3.3mm). This is consistent with the fact that the ratio of resistivity of ITO/Au is over 20. These results suggest that the accuracy and sensitivity of the AE hydrophone depends largely on the shape and resistivity of the device.

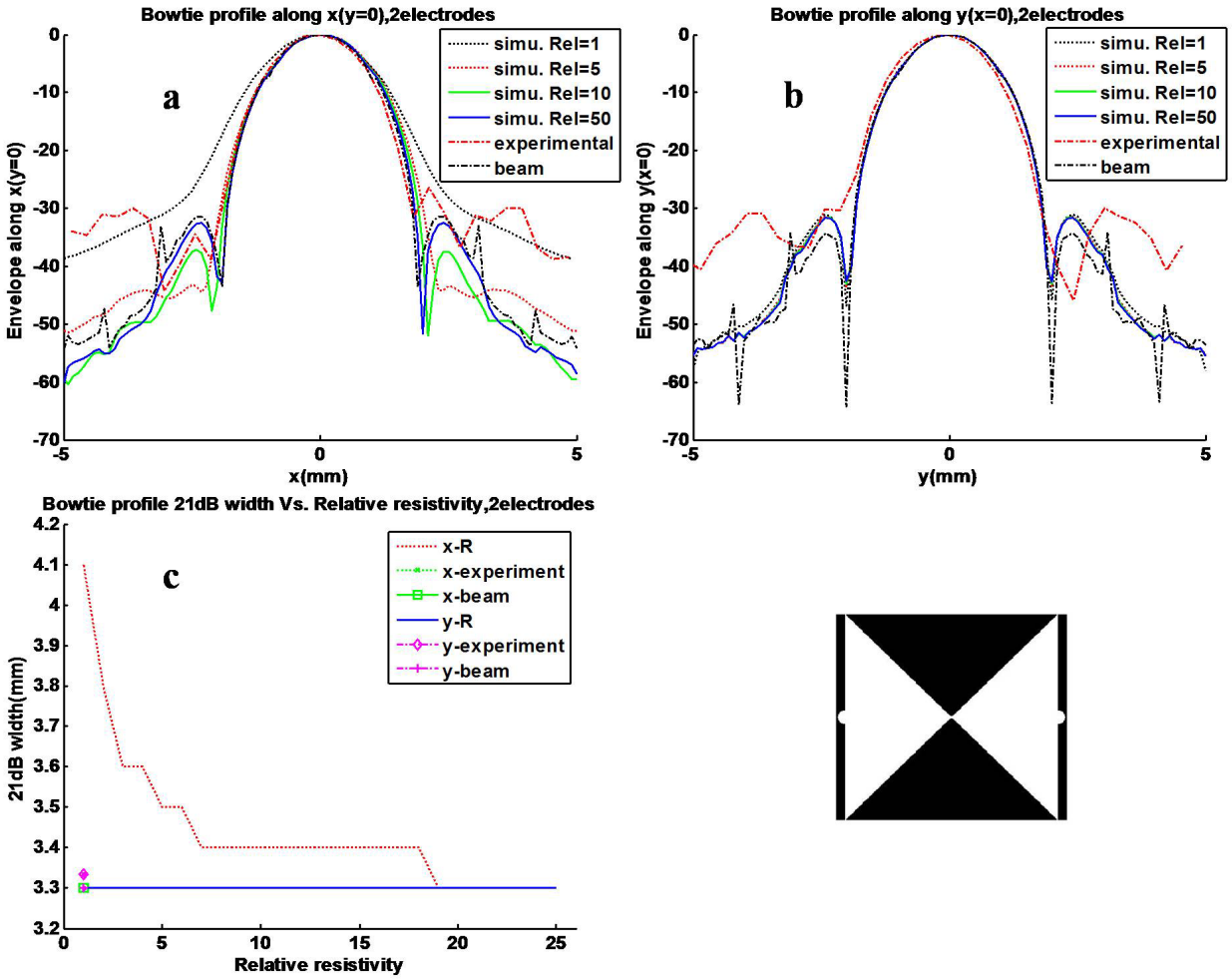

Figure 10. The effect of the relative resistivity of ITO/gold (Au) over the AE bowtie (triangular) hydrophone beam pattern. 'Experimental' is from the experimental data of bowtie hydrophone with ITO on the 200μm*200μm center and gold on the rest parts. 'Beam' is the transducer beam pattern on the focus simulated by FIELD II, 'Simu. Rel' is the simulated AE signal on the focus with different relative resistivity of ITO/Au. (a) Profile on the center along x direction, where 'experimental' has -30dB sidelobe caused by reflected noise, Rel=1 has the highest sidelobe and biggest full width at half maximum (FWHM), but when Rel increases higher, the AE profile converges to the transducer 'beam' pattern. In (b), each profile of simulated AE signals with different Rel value has almost the same shape of transducer 'beam' pattern along y direction. The experimental data within [-3, 3]mm is close to transducer 'beam' pattern, but the noise is high out of that range. (c) is to determine the lowest relative resistivity of ITO/Au that can realize the ideal or experimental result. 'x(y)-R' is the beam width at 21dB along x(y) direction for simulated hydrophones with different relative resistivity. 'x(y)-experiment' is the beam width at 21dB along x(y) direction for real ITO/Au hydrophone. 'x(y)-beam' is the beam width at 21dB along x(y) direction for simulated transducer beam pattern, created by the convolution of ultrasound field with AE signals obtained by the Onda hydrophone. At 21dB, if the relative resistivity of ITO/Au is higher than 18, the beam width (3.3mm,'x-R') becomes equivalent to the experimental result (3.3mm, 'x-experiment'). Relative resistivity of ITO/Au does not affect the center profile or beam width along y direction.

4. CONCLUSION

The computational efficiency of simulation is highly improved by multiple dimensional Fourier and inverse Fourier transform, so that the AE hydrophone can be simulated within short period. The shape and relative resistivity are both important for design high performance acousto-electric hydrophone. The AE hydrophone with a dumbbell configuration achieved the best beam pattern of a 2.25MHz ultrasound transducer with lateral and axial resolutions consistent with images generated from a commercial hydrophone (Onda Inc.). A bowtie shape with high relative resistivity can realize

high performance of mapping, and it is easier to make bowtie shape than to create a clean long thin gap for dumbbell hydrophone, especially tiny size about several μm for high frequency transducer. The higher the relative resistivity is, the stronger AE signal is detected, and the performance of hydrophone is better.

Therefore, optimization of the AE hydrophone can be enhanced with simulations of the electric resistivity of the device combined with the ultrasound beam. Prototypes based on these simulations support these initial results. We anticipate that optimizing the design of these inexpensive and durable AE hydrophones will lead to new devices for applications in ultrasound imaging and therapy.

5. ACKNOWLEDGMENTS

This study was supported by grants NIH (R01EB009353), Technology and Research Initiative Fund (TRIF) and Advanced Research Institute for Biomedical Imaging (ARIBI).

6. REFERENCES

[1] Haider, S., Hrbek, A., and Xu, Y., "Magneto-acousto-electrical tomography: a potential method for imaging current density and electrical impedance," Physiological Measurement, 29, S41–S50 (2008)

[2] Olafsson, R., Witte, R.S., Huang, S.W., and O'Donnell, M., "Ultrasound Current Source Density Imaging", IEEE Transactions On Biomedical Engineering 50(7), 1840-1848 (2007)

[3] Malmivuo, J., Plonsey, R., [Bioelectromagnetism], Oxford University Press Inc., New York, chapters 6 & 11 (1995)

[4] Wang, Z., Ingram, P., Olafsson, R., Li, Q., and Witte, R.S., "Detection of Multiple Electrical Sources in Tissue Using Ultrasound Current Source Density Imaging," Medical Imaging 2010, Proceedings of SPIE 7629, 762916 in press (2010)

[5] Witte, R.S., Hall, T., Olafsson, R., Huang, S.W., and O'Donnell, M., "Inexpensive acoustoelectric hydrophone for mapping high intensity ultrasounic fields", Journal of Applied Physics 104, 054701 (2008)

[6] Ingram, P., Greenlee, C., Wang, Z., Olafsson, R., Norwood, R., Witte, R.S., "Fabrication and characterization of an indium tin oxide acoustoelectric hydrophone," Proceedings of SPIE 7629, 762923 in press (2010)

[7] Jensen, J. A., Svendsen, N. B., "Calculation of Pressure Fields from Arbitrarily Shaped, Apodized, and Excited Ultrasound Transducers," IEEE Transactions On Ultrasonics, Ferroelectrics, and Frequency Control, 39(2), 262-267 (1992)

[8] Jensen, J. A., Munk P., "Computer Phantoms For Simulating Ultrasound B-mode And Cfm Images," 23rd Acoustical Imaging Symposium, Boston, Massachusetts, USA (1997)